Energy Deposition in S_N2 Reaction Products and Kinetic Energy Effects on Reactivity

Jianhua Ren and John I. Brauman*

Department of Chemistry, Stanford University, Stanford, California 94305-5080

Received: November 8, 2001; In Final Form: January 9, 2002

Translational energy dependence of reaction kinetics and internal energy depositions in reaction products were examined for gas-phase S_N2 reactions of Cl^- and F^- with $NCCO_2CH_3$ and $CF_3CO_2CH_3$ in a Fourier transform ion cyclotron resonance mass spectrometer (FTICR). The energy dependence of the kinetics was examined by measuring the S_N2 rate constants as a function of reactant ion translational energies and by comparing the experimental results with those calculated using RRKM theory. Negative kinetic energy dependence was observed, and the changes of rate constants agree with RRKM theory predictions. The internal energy deposition in the S_N2 products was examined by measuring the fraction of secondary fragments resulting from dissociation of the ionic S_N2 product. A statistical model was used to calculate the statistical fraction of internally excited S_N2 product ion under thermal conditions. For the least exothermic reaction (<20 kcal/mol), the measured fraction of secondary ion is comparable to the statistical fraction of internally excited ionic product. For a highly exothermic reaction (>40 kcal/mol), the internal energy deposition in the ionic S_N2 product is significantly lower than the statistical value, indicating that most of the excess energy is trapped in the neutral product. Additional translational energy has little effect on the observed fractions of secondary ions.

Introduction

Gas-phase S_N2 reactions have been an important object of study for more than two decades.[1] Both experimental and theoretical studies suggest that a gas-phase S_N2 reaction can be characterized by a double-well potential energy surface with a central barrier separating two ion−molecule complexes.[2−9] A generalized double-well potential energy surface is shown in Figure 1. The reaction kinetics are often modeled with statistical theories such as Rice−Ramsperger−Kassel−Marcus (RRKM) theory or phase space theory (PST).[10−13] Despite the general use of statistical theories in interpreting the results of reaction kinetics, there are fundamental questions regarding the validity of statistical models.[14−16] How does the collision energy affect the reactivity? Does the change in reaction rates agree with statistical theory predictions at increasing collision energies? For an exothermic reaction, how is the exothermicity distributed in the reaction products? Is the energy distributed statistically over all available internal modes of the two products, or is the energy preferentially partitioned into one product?

Most ion−molecule complexes have relatively large association energies. Therefore, it is not unreasonable to assume that the complex is long-lived, and the energy redistribution within the complex is statistical, so that the reaction kinetics can be described with a statistical theory, and the energy distribution in reaction products can be calculated using a statistical model. Many experimental and theoretical studies have been carried out to investigate whether S_N2 reactions behave statistically.[17−29] Most experimental studies focus on examination of reaction kinetics with energy perturbations.[18,19,24,26,30−32] In general, for small systems (such as $Cl^- + CH_3Br$), reaction kinetics behave nonstatistically,[18] while for relatively large systems (such as $Cl^- + NCCH_2Cl$), energy-dependence kinetics agree with RRKM theory predictions.[26,33] Extensive trajectory simulations on small systems, $Cl^- + CH_3Br$ for example, show weak coupling between relative translational modes (of Cl^- and CH_3Br) and vibrational modes (of CH_3Br).[21,22] This weak coupling would inhibit energy flow within the ion−molecule complex and result in nonstatistical behavior in the reaction kinetics. Simulations also show that the reaction products tend to have lower translational and rotational energy but higher vibrational energy distributions compared to the values predicted by a statistical model.[23]

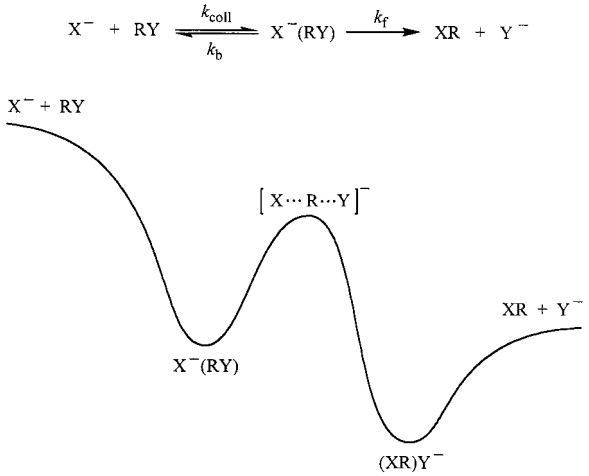

Figure 1. Generalized S_N2 potential energy surface.

There have been experimental studies of translational energy distributions in S_N2 products.[34−37] The kinetic energy release distribution (KERD) experiments of dissociation of metastable ions,[34−36] including $[(CH_3Br)Cl^-]^*$ and $[(CF_3CO_2CH_3)Cl^-]^*$, revealed that the relative kinetic energy distributions in the displacement products were significantly lower than those predicted by the statistical phase space theory. The results indicate that the energies generated in these reactions were

* Corresponding author. E-mail: brauman@stanford.edu.

10.1021/jp0141070 CCC: $22.00
Published on Web 03/20/2002

trapped in the vibrational modes of the products rather than distributed statistically between the vibrational and the translational degrees of freedom.

It is of interest to examine whether internal (vibrational) energy distributions in S_N2 products behave statistically. These distributions have not previously been examined. In this contribution, we report a method to estimate internal energy deposition in S_N2 reaction products by measuring the fraction of the secondary fragments resulting from dissociation of the ionic S_N2 product. For a generic gas-phase S_N2 reaction (eq 1), the ionic product, Y^-, can further dissociate to give the secondary fragment ion, A^- (eq 1a). Only those Y^- having excess internal energy above the dissociation threshold will fragment and produce A^-. Thus, the fraction of A^- formed indicates the fraction of Y^- having internal energy above the critical energy for dissociation. We have developed a statistical model to calculate the statistical energy deposition in reaction products. By comparing the measured fraction of A^- with that calculated by using the statistical model, we examine whether the energy deposition in Y^- behaves statistically. Furthermore, we examine additional kinetic energy deposition by measuring the fraction of A^- as a function of the increase in the translational energy of X^-. Our results show that for the reactions studied the reaction energy is preferentially deposited in the neutral products.

$$X^- + RY \rightarrow XR + Y^- \quad (1)$$

$$Y^- \rightarrow A^- + B \quad (1a)$$

We also report an investigation of translational energy dependence on reaction kinetics by measuring the changes of reaction rates as a function of the increase in reactant ion translational energy and by comparing the results with those calculated using RRKM theory.

Experimental Section

Instrumentation. Experiments were carried out in an IonSpec OMEGA Fourier transform ion cyclotron resonance mass spectrometer (FTICR) equipped with an ion kinetic energy controller.[14,38,39] Details of the apparatus have been described elsewhere. The instrument is operated at a 0.6 T magnetic field with a background pressure of 3×10^{-9} Torr. The temperature in the ICR cell was estimated to be 350 K.[40] Neutral reagents were added to the vacuum chamber through variable-leak valves. The pressure of the neutral reagents was measured with a Varian ionization gauge calibrated against an MKS Baratron capacitance manometer. The primary ions were generated by electron impact, and the unwanted ions were removed by ejection signals. Impulse excitation was used to excite the ions prior to detection.[41] All chemicals were purchased from Aldrich and were used without further purification. Multiple freeze−pump−thaw cycles were applied to all the gaseous and liquid chemicals prior to their introduction into the vacuum chamber.

The function of the ion kinetic energy controller is to supply a 180° phase-shifting radio frequency (rf) with variable voltage to the selected ion so that the ion can be accelerated and trapped in the ICR cell for about 2 s.[38] In a fixed electrical field, ions are accelerated as they undergo N cyclotron cycles, and at the end of N periods, the phase of the rf signal is reversed by 180° and the ions are then decelerated for another N cycles. The cycle is then repeated. Thus, the maximum translational energy of an ion[42,43] can be varied simply by changing the value of N. In the absence of collisions, a particular ion would oscillate between the same minimum and maximum radii indefinitely.[44] Under ion collisions with neutral molecules, the ion minimum and maximum positions are displaced with respect to the phase shifts of the driving signal.[45] In addition, collisions serve to decrease the kinetic energy of an ion. Under the condition that the delay time is long relative to the collision time scale, the kinetic energy distribution of ions can be determined by summing over the trajectories of the ions under thermalizing collisions at a random time in the acceleration/deceleration interval.[45]

Experiments. The reactant ion, Cl^- or F^-, was generated by electron impact on CCl_4 or NF_3, respectively. The neutral reagent, $NCCO_2CH_3$ or $CF_3CO_2CH_3$, was introduced into the vacuum chamber through a leak valve, and the pressure of the neutral reagent was in the range of $(1.5-2.5) \times 10^{-7}$ Torr. It was found that by adding argon as a buffer gas (4×10^{-7} Torr) the ion signals were more stable and more reproducible. The electron ejection gate was opened at 40 ms to remove extra electrons. If $^{35}Cl^-$ was the reactant ion, then the isotopic ion $^{37}Cl^-$ was removed with an ejection pulse immediately after the ion was formed. To remove other ions generated by electron impact on the neutral reagents, all of the ions except the reactant ion (Cl^- or F^-) were ejected 50−60 ms after opening the electron ejection gate. Immediately after the other ions were ejected, the gate of the kinetic energy controller was opened, and an on-resonance (±10 Hz) rf signal was applied to accelerate the selected ion. The peak-to-peak voltage of the rf signal was in the range of 0.032 to 0.1 V, corresponding to an electrical field of 0.64 to 2 V/m. The interval between the phase shifts was in the range of $N = 40-240$ cycles. The applied rf pulse lasted 200−1000 ms, and the impulse excitation signal was applied 50 ms after turning off the rf signal. It was found that the product ions formed within the 50 ms were negligible compared to those formed under the rf driving signal.

Differential ion loss is a major concern when an rf signal is applied.[46] Control experiments were performed for each set of experiments. If $^{35}Cl^-$ was the ion to be accelerated, then the nonreactive CCl_4 was used as the test reagent. Both chloride isotopes were generated by electron impact. An on-resonance rf signal was applied to $^{35}Cl^-$ at a fixed rf potential, and the number (N) of acceleration cycles was varied. The isotopic ratio was monitored between 100 and 1000 ms of acceleration time. When a 10% loss of differential ions was observed, the rf potential and N cycles were set as the upper limits. If F^- was the ion being accelerated, then the mixture of CCl_4 and NF_3 was used as the test reagent, and the ratio of F^- and Cl^- was monitored. We found that by using suitable trapping potentials (2.5−3.5 V) differential ion loss during the acceleration period can be minimized significantly.

The fractions of secondary ions and the reaction rate constants were measured in the following manner. Under thermal conditions, the intensities of Y^- and A^- (eq 1 and 1a) were monitored at several different time increments until a constant branching ratio was reached (say, at 500 ms). Then the intensities of the product ions were recorded. To measure the fraction of secondary product as a function of the increase in reactant ion translational energy, an on-resonance rf signal was applied to X^-, and the intensities of Y^- and A^- were detected at 500 ms (the same as that for the thermal condition). The fraction (F_{expt}) of A^- is

$$F_{expt} = \frac{[A^-]}{[A^-] + [Y^-]} \quad (2)$$

To obtain rate constants at different translational energies of X^-, the absolute intensities of X^- were measured as a function of time while X^- was accelerated by an rf signal. The rate constant, k, was given by eq 3, where C is a constant and n is the number density (in molecules cm^{-3}) of the neutral reactant, RY.

$$\ln[Y^-] = n \cdot k \cdot t + C \tag{3}$$

Quantum Calculations.[47] The structures and vibrational frequencies for the neutral molecules, ions, and ion−molecule complexes were calculated using the B3LYP/6-31G(d) procedure. Transition states were located on the B3LYP potential energy surfaces by using the QST3 method. The initial-guess transition state structures were obtained by scanning the potential energy as a function of the distance between the nucleophile and the reaction center. True energy minima and saddle points were confirmed by frequency analysis and by viewing the motion of the structure corresponding to each vibrational mode. For all the structures at the energy minima, no imaginary frequencies were found. For each of the transition state structures, one imaginary frequency was found. The reaction energies were obtained by performing single-point calculations at the MP2 level with the 6-311+G(2d,p) basis set. For comparison, the reaction energies were also calculated by using the MP2/6-311+G(2d,p)//HF/6-31+G(d) and the CBS-4 procedures. The calculated results were compared with the available experimental data. Detailed geometrical information, energies, vibrational frequencies, and rotational constants are provided in the Supporting Information.

Statistical and Kinetic Modeling. We used a statistical model to calculate the probabilities of energy distribution in S_N2 reaction products. For the generic S_N2 reaction (eq 1), the total energy generated from the reaction is E. The energy deposited in Y^- is E_1, and in RX, $E - E_1$. The probability[48] of energy distribution in Y^- is given by eq 4, where $\rho(E_1)$ is the density of states for Y^- at energy E_1 and $\rho(E - E_1)$ is the density of states for RX at energy $(E - E_1)$. The density of states was calculated using the Beyer−Swinehart direct-count algorithm.[49] Only vibrational contributions were considered in the calculations; we assume that the rotational contributions are sufficiently small to be neglected. The vibrational frequencies were calculated by using the B3LYP/6-31G(d) computational procedure. If S_1 and S_2 represent the amounts of Y^- having energy above and below the critical energy for dissociation, respectively, then the fraction of Y^- having energy above the critical energy is given by eq 5.

$$P = \frac{\rho(E_1)\,\rho(E - E_1)}{\int \rho(E_1)\,\rho(E - E_1)\,\mathrm{d}E_1} \tag{4}$$

$$F_{\mathrm{stat}} = \frac{S_1}{S_1 + S_2} \tag{5}$$

We model the reaction kinetics with a double-well potential energy surface (Figure 1) y using the RRKM program HYDRA.[50] The overall S_N2 rate (k_{obs}) can be related to the ion−molecule collision rate (k_{coll}) and the rates of unimolecular dissociation back to reactants (k_b) and isomerization (k_f) (eq 6).

$$k_{\mathrm{obs}} = k_{\mathrm{coll}} \frac{k_{\mathrm{f}}}{k_{\mathrm{f}} + k_{\mathrm{b}}} \tag{6}$$

A more convenient representation of this relation is to replace the $k_f/(k_f + k_b)$ term with the macroscopic efficiency of the reaction, Φ, the fraction of collisions that lead to product formation. The observed rate constant is then described as the collision rate constant multiplied by the reaction efficiency (eq 7).

$$k_{\mathrm{obs}} = k_{\mathrm{coll}}\Phi \tag{7}$$

The macroscopic efficiency is the integration of the microscopic counterparts, $\Phi(E,J)$ (eq 8), weighted according to the thermal equilibrium energy and angular momentum distribution of the reactant complex, $F(E,J)$. Each microscopic $\Phi(E,J)$ is the fraction of collisions with energy E and angular momentum J that leads to product formation (eq 9), in which the unimolecular rate constants, $k_f(E,J)$ and $k_b(E,J)$, are calculated using the μVTST-RRKM formalism described in a previous paper.[5] To model a system at increased translational energy, the added translational energy is assumed to be incorporated into the internal modes of the reactant complex. Therefore, the average total energy of the system is equal to the average thermal energy (350 K) of the reactants plus the center-of-mass (CM) collision energy. The temperature of the system is replaced with an effective temperature (T_{eff}) corresponding to a temperature at which the collision complex has a Boltzmann distribution of the total internal energy.

$$\Phi = \int\int \Phi(E, J)\, F(E, J)\, \mathrm{d}E\, \mathrm{d}J \tag{8}$$

$$\Phi(E, J) = \frac{k_{\mathrm{f}}(E, J)}{k_{\mathrm{f}}(E, J) + k_{\mathrm{b}}(E, J)} \tag{9}$$

The collision rate constant, k_{coll}, is calculated using the parametrized Su trajectory model, in which the relative kinetic energy of the system is a variable.[51] The average center-of-mass kinetic energy of the reactant ion is obtained from trajectory calculations of ions undergoing reversible rf acceleration.[45]

Results

Four gas-phase S_N2 reactions (eqs 10−13) with different exothermicities and different secondary dissociation energies were chosen for this study. The product ions, $NCCO_2^-$ (eq 14) and $CF_3CO_2^-$ (eq 15), can decompose further to give secondary fragments, CN^- and CF_3^-, with dissociation energies of 17.3 and 39.8 kcal/mol,[52,53] respectively.

$$CF_3CO_2CH_3 + Cl^- \rightarrow CF_3CO_2^- + CH_3Cl \qquad \Delta H^\circ = -16 \text{ kcal/mol} \tag{10}$$

$$\rightarrow CF_3^- + CO_2 + CH_3Cl \qquad \Delta H^\circ = +23 \text{ kcal/mol} \tag{10a}$$

$$NCCO_2CH_3 + Cl^- \rightarrow NCCO_2^- + CH_3Cl \qquad \Delta H^\circ = -20 \text{ kcal/mol} \tag{11}$$

$$\rightarrow CN^- + CO_2 + CH_3Cl \qquad \Delta H^\circ = -3 \text{ kcal/mol} \tag{11a}$$

$$CF_3CO_2CH_3 + F^- \rightarrow CF_3CO_2^- + CH_3F \quad \Delta H^\circ = -47 \text{ kcal/mol} \quad (12)$$

$$\rightarrow CF_3^- + CO_2 + CH_3F \quad \Delta H^\circ = -8 \text{ kcal/mol} \quad (12a)$$

$$NCCO_2CH_3 + F^- \rightarrow NCCO_2^- + CH_3F \quad \Delta H^\circ = -50 \text{ kcal/mol} \quad (13)$$

$$\rightarrow CN^- + CO_2 + CH_3F \quad \Delta H^\circ = -23 \text{ kcal/mol} \quad (13a)$$

$$NCCO_2^- \rightarrow CN^- + CO_2 \quad \Delta H^\circ = 17.3 \text{ kcal/mol} \quad (14)$$

$$CF_3CO_2^- \rightarrow CF_3^- + CO_2 \quad \Delta H^\circ = 39.8 \text{ kcal/mol} \quad (15)$$

We measured rate constants and reaction efficiencies for the four S_N2 reactions. We studied the kinetic energy dependence on reactivity for reactions 10 and 11, and we examined internal energy distributions in S_N2 products for reactions 11−13.

Experimental Results

Cl^- with $CF_3CO_2CH_3$ (eq 10) generated only one ionic product, $CF_3CO_2^-$. No secondary fragment was observed by adding up to 12 kcal/mol (CM) of translational energy to the Cl^- ion. The thermal-reaction rate constant, 1.0×10^{-10} cm^3 molecule^{-1} s^{-1}, was determined by measuring the decay of Cl^- as a function of time. The collision rate constant for $Cl^- + CF_3CO_2CH_3$ was calculated[51] to be 2.8×10^{-9} cm^3 molecule^{-1} s^{-1}, giving a reaction efficiency of 0.037 at thermal energy (Table 1). The rate constants at increasing Cl^- kinetic energies were measured by applying on-resonance rf signals to the Cl^- ion by using the ion kinetic energy controller described in the Experimental Section. The reaction rate decreases as the kinetic energy increases, Figure 2a.

Cl^- with $NCCO_2CH_3$ (eq 11) yielded three ionic products: $NCCO_2^-$ (78%, the S_N2 product), CN^- (12%), and $(NCCO_2CH_3)$-CN^- (10%). The ion CN^- most likely comes from dissociation of $NCCO_2^-$. The addition−elimination reaction (eq 16) is estimated to be endothermic by 18 kcal/mol (Table 4), and CN^- would not be observed from this reaction. The ion $(NCCO_2CH_3)$-CN^- arises from the reaction of $NCCO_2^-$ with the neutral reactant, $NCCO_2CH_3$ (eq 17).

$$NCCO_2CH_3 + Cl^- \rightarrow CN^- + ClCO_2CH_3 \quad (16)$$

$$NCCO_2CH_3 + NCCO_2^- \rightarrow (NCCO_2CH_3)CN^- + CO_2 \quad (17)$$

The S_N2-reaction rate constant (7.5×10^{-10} cm^3 molecule^{-1} s^{-1}) was determined by measuring the decay of Cl^- as a function of time. Combined with the calculated collision rate constant (3.9×10^{-9} cm^3 molecule^{-1} s^{-1}), the S_N2 reaction efficiency was determined to be 0.19 (Table 1). By applying on-resonance rf signals to Cl^-, we measured the S_N2-reaction rate constants at higher kinetic energies. The measured rate constant as a function of the increase in collision energies is shown in Figure 2b.

Under thermal conditions, the fraction of CN^- relative to the total amount of $NCCO_2^-$ produced from the S_N2 reaction is 0.12 (Table 2). To examine whether additional kinetic energy has an effect on the dissociation of $NCCO_2^-$, we measured the fraction of CN^- as the Cl^- was accelerated by the on-resonance rf signals. A 20% increase in the fraction of CN^- was observed by adding 4.7 kcal/mol (CM) of kinetic energy to the Cl^- ion (Figure 3a).

TABLE 1: Reaction Rate Constants, Collision Rate Constants, and Efficiencies Determined at Thermal Energy

reactants	k_{obs} (10^{-9} cm^3 molecule^{-1} s^{-1})	k_{coll}[a] (10^{-9} cm^3 molecule^{-1} s^{-1})	Φ
$CF_3CO_2CH_3 + Cl^-$	0.11	2.8	0.037
$NCCO_2CH_3 + Cl^-$	0.75	3.9	0.19
$CF_3CO_2CH_3 + F^-$	3.0	3.7	0.82
$NCCO_2CH_3 + F^-$	4.3	4.9	0.87

[a] Calculated using the Su trajectory model, ref 51.

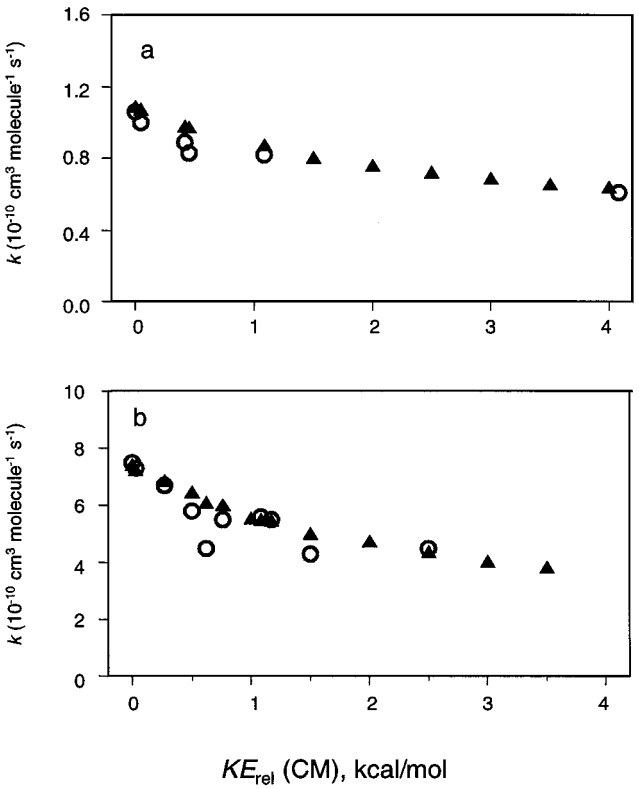

Figure 2. Experimental (○) and RRKM (▲) rate constants vs relative kinetic energies. (a) $Cl^- + CF_3CO_2CH_3$. (b) $Cl^- + NCCO_2CH_3$.

TABLE 2: Fractions of Secondary Fragments (F_{expt}) Determined at Thermal Energy and Fractions of Internally Excited Ionic S_N2 Products (F_{stat}) Expected from the Statistical Model

reactants	F_{expt}	F_{stat}
$CF_3CO_2CH_3 + Cl^-$	0	0
$NCCO_2CH_3 + Cl^-$	0.12	0.18
$CF_3CO_2CH_3 + F^-$	0.01	0.34
$NCCO_2CH_3 + F^-$	0.4	0.94

F^- with $CF_3CO_2CH_3$ (eq 12) generated one major product ion $CF_3CO_2^-$ and a trace (1%) of CF_3^-. The corresponding addition−elimination reaction (similar to eq 16) is endothermic by 8 kcal/mol, and formation of CF_3^- from eq 12 is exothermic by 8 kcal/mol (Table 4). Therefore, the observed CF_3^- is most likely the result of the dissociation of $CF_3CO_2^-$. Combining the measured rate constant of 3.0×10^{-9} cm^3 molecule^{-1} s^{-1} and the calculated collision rate constant of 3.7×10^{-9} cm^3 molecule^{-1} s^{-1}, the reaction efficiency is 0.82 (Table 1).

We examined the formation of CF_3^- at increasing F^- translational energies. The observed fractions of CF_3^- (0.01 at

TABLE 3: Reaction Energies (298 K) Obtained from Quantum Mechanical Calculations and Experimental Heats of Formation

reactions	MP2/6-311+G(2d,p)//HF/6-31G(d), kcal/mol	MP2/6-311+G(2d,p)//B3LYP/6-31G(d), kcal/mol	CBS-4, kcal/mol	expt,[a] kcal/mol
$CF_3CO_2CH_3 + Cl^- \rightarrow CF_3CO_2^- + CH_3Cl$	−11.7	−9.9	−10.3	−16.5
$NCCO_2CH_3 + Cl^- \rightarrow NCCO_2^- + CH_3Cl$	−17.2	−16.3	−19.7	
$CF_3CO_2CH_3 + F^- \rightarrow CF_3CO_2^- + CH_3F$	−41.6	−40.5	−36.8	−47.5
$NCCO_2CH_3 + F^- \rightarrow NCCO_2^- + CH_3F$	−47.4	−46.9	−46.2	
$NCCO_2^- \rightarrow CN^- + CO_2$	+15.7	+15.4	+20.0	+16.7[b]
$CF_3CO_2^- \rightarrow CF_3^- + CO_2$	+38.9	+38.9	+43.2	+39.2

[a] Derived from experimental heats of formation, ref 53. [b] Experimental data, ref 52.

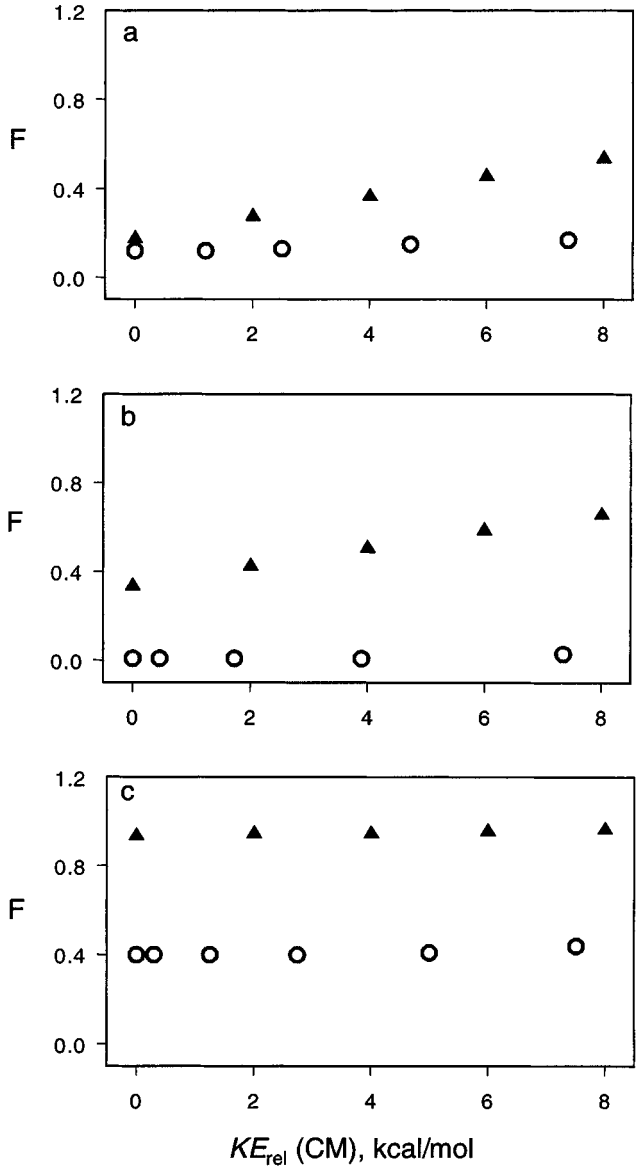

Figure 3. F_{expt} (○) and F_{stat} (▲) vs relative kinetic energies. (a) $Cl^- + NCCO_2CH_3$. (b) $F^- + CF_3CO_2CH_3$. (c) $F^- + NCCO_2CH_3$.

thermal energy, Table 2) are essentially unchanged by adding up to 7 kcal/mol (CM) of kinetic energy to the F^- ion (Figure 3b).

F^- with $NCCO_2CH_3$ (eq 13) produced two ionic products, $NCCO_2^-$ and CN^-, in the ratio of 60:40. A trace (<3%) of $(NCCO_2CH_3)CN^-$ was formed from the reaction of $NCCO_2^-$ with the neutral reactant $NCCO_2CH_3$ (eq 17). Formation of CN^- from dissociation of the S_N2 product, $NCCO_2^-$ (eq 13a), is exothermic by 23 kcal/mol. The addition−elimination reaction of F^- with $NCCO_2CH_3$ (eq 18) was estimated to be exothermic by 21 kcal/mol (Table 4). Thus, both reactions 13a and 18 could contribute to the observed CN^-. The product ion ratio is also complicated by the reaction of CN^- with $NCCO_2CH_3$, which would give back $NCCO_2^-$ (eq 19).[52] With continuing ejection of CN^-, the intensity of $NCCO_2^-$ decreased to 50% of the total product ion, suggesting that the maximum amount of CN^- formed from this system would be 50%. We used the observed value of 40% of CN^- for our data analysis.

$$NCCO_2CH_3 + F^- \rightarrow CN^- + FCO_2CH_3 \qquad (18)$$

$$NCCO_2CH_3 + CN^- \rightarrow NCCO_2^- + CH_3CN \qquad (19)$$

The overall rate constant for the reaction of F^- with $NCCO_2CH_3$ was measured to be 4.3×10^{-9} cm^3 molecule^{-1} s^{-1}. The ion−molecule collision rate constant was calculated to be 4.9×10^{-9} cm^3 molecule^{-1} s^{-1}, giving a reaction efficiency of 0.87 (Table 1).

The thermal fraction of CN^- arising from dissociation of $NCCO_2^-$ is 0.4 (Table 2). The observed fraction of CN^- increases slightly (10%) by adding 7 kcal/mol (CM) of kinetic energy to the F^- ion. The fraction of CN^- as a function of the increase in F^- translational energy is plotted in Figure 3c.

Computational Results

The calculated reaction thermochemistry along with available experimental data is summarized in Table 3. On the basis of heats of formation,[53] the 298 K energies for reactions 10 and 12 were estimated to be −16.5 and −47.5 kcal/mol, respectively. The energies for reaction 10 calculated by using the three computational methods MP2/6-311+G(2d,p)//HF/6-31G(d) (−11.7 kcal/mol), MP2/6-311+G(2d,p)//B3LYP/6-31G(d) (−9.9 kcal/mol), and CBS-4 (−10.3 kcal/mol) are in good agreement with each other but are about 4 kcal/mol higher than the derived experimental value (−16.5 kcal/mol). The energies for reaction 12 calculated at the MP2/6-311+G(2d,p)//HF/6-31G(d) (−41.6 kcal/mol) and MP2/6-311+G(2d,p)//B3LYP/6-31G(d) (−40.5 kcal/mol) levels are in good agreement with each other but are about 5 kcal/mol higher than the derived experimental value (−47.5 kcal/mol). The CBS-4 method gives a somewhat higher value (−36.8 kcal/mol). Considering 3 kcal/mol of uncertainty, the reaction energies calculated with MP2/6-311+G(2d,p)//HF/6-31G(d) and MP2/6-311+G(2d,p)//B3LYP/6-31G(d) are about 3 kcal/mol higher than the values derived from the heats of formation for reactions 10 and 12. We added 3 kcal/mol of energy as a correction factor for reactions 11 and 13. The energies for reactions 11 and 13 cannot be derived from heats of formation because the heat of formation for $NCCO_2CH_3$ is unknown. The two computational methods, MP2/6-311+G(2d,p)//HF/6-31G(d) (−17.2 kcal/mol) and MP2/6-311+G(2d,p)//B3LYP/6-31G(d) (−16.3 kcal/mol), predicted an average of −17 kcal/mol for the energy of reaction 11. By adding the 3 kcal/mol correction factor, we estimated the energy for

TABLE 4: Reaction Energies Calculated Using the MP2/6-311+G(2d,p)//B3LYP/6-31G(d) Method

reaction	energy, kcal/mol (298 K)
$CF_3CO_2CH_3 + Cl^- \rightarrow CF_3^- + CO_2 + CH_3Cl$	23
$CF_3CO_2CH_3 + Cl^- \rightarrow CF_3^- + ClCO_2CH_3$	47.9
$NCCO_2CH_3 + Cl^- \rightarrow CN^- + CO_2 + CH_3Cl$	−3
$NCCO_2CH_3 + Cl^- \rightarrow CN^- + ClCO_2CH_3$	18.06
$CF_3CO_2CH_3 + F^- \rightarrow CF_3^- + CO_2 + CH_3F$	−8
$CF_3CO_2CH_3 + F^- \rightarrow CF_3^- + FCO_2CH_3$	8.09
$NCCO_2CH_3 + F^- \rightarrow CN^- + CO_2 + CH_3F$	−23
$NCCO_2CH_3 + F^- \rightarrow CN^- + FCO_2CH_3$	−21.76

reaction 11 to be −20 kcal/mol, which is about the same as the value (−19.7 kcal/mol) obtained with the CBS-4 method. Similarly, calculations from the three computational methods, MP2/6-311+G(2d,p)//HF/6-31G(d) (−47.4 kcal/mol), MP2/6-311+G(2d,p)//B3LYP/6-31G(d) (−46.9 kcal/mol), and CBS-4 (−46.2 kcal/mol), gave a value of −47 kcal/mol for reaction 13. By adding the 3 kcal/mol correction factor, we estimate the energy for reaction 13 to be −50 kcal/mol.

The enthalpy change for the dissociation of $NCCO_2^-$ was reported to be 17.3 kcal/mol,[52] corresponding to an energy change of 16.7 kcal/mol for this dissociation. The dissociation energy for $CF_3CO_2^-$ was derived to be 39.2 kcal/mol from the available heats of formation.[53] The dissociation energies for $NCCO_2^-$ and $CF_3CO_2^-$ calculated by using both the MP2/6-311+G(2d,p)//HF/6-31G(d) (15.7 and 38.9 kcal/mol) and the MP2/6-311+G(2d,p)//B3LYP/6-31G(d) (15.4 and 38.9 kcal/mol) methods are in good agreement with the experimental results, 16.7 and 39.2 kcal/mol, respectively. The CBS-4 method gives about a 3 kcal/mol higher value for both species.

To estimate the possibility of forming another isomeric product complex, $[(CN-CO_2^-)CH_3Cl]$ (the N−C isomer) in reaction 11, we calculated the structure and the energy of this isomer at the MP2/6-311+G(2d,p)//B3LYP/6-31G(d) level. This isomer was found to be 16 kcal/mol higher in energy than the corresponding C−C isomer, $[(NC-CO_2^-)CH_3Cl]$, at the same level of calculation. Therefore, the product complex in reaction 11 most likely has the form of $[(NCCO_2^-)CH_3Cl]$, and CN^- most likely comes directly from dissociation of $NCCO_2^-$.

We also calculated the energies of the addition−elimination reactions and the energies of formation of the secondary fragments from the four S_N2 reactions at the MP2/6-311+G(2d,p)//B3LYP/6-31G(d) level. The results are summarized in Table 4.

Statistical Modeling

A. Kinetics. The statistical rate constants for reactions 10 and 11 as a function of the increase in the reactant ion translational energies were modeled with the RRKM program, HYDRA, described in the Experimental Section. For RRKM calculations, the vibrational frequencies and the rotational constants of the related molecules and ions were obtained from B3LYP/6-31G(d) calculations. The relative energies of the reactants, products, and intermediate complexes on the potential energy surfaces were calculated by using the MP2/6-311+G(2d,p)//B3LYP/6-31G(d) procedure. The well depths of the entrance and exit channels for reaction 10 are 11.7 and 8.6 kcal/mol, respectively, and for reaction 11 are 14.5 and 7.0 kcal/mol, respectively. The central barrier heights of the potential energy surfaces were determined by fitting the calculated statistical efficiency ($\Phi = k_f/(k_f + k_b)$) with the observed efficiencies ($\Phi = k_{obs}/k_{coll}$) at thermal energies. The experimental efficiencies for reactions 10 and 11 are 0.037 and 0.19, respectively (Table 1). The barrier heights relative to those of the reactant complexes were determined to be 8.6 and 8.2 kcal/mol, corresponding to activation energies of −3.1 and −6.3 kcal/mol for reactions 10 and 11, respectively.

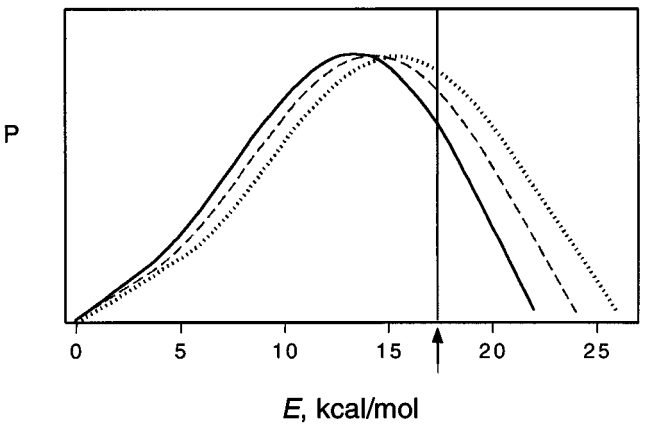

Figure 4. Probability, P, of energy distributions in $NCCO_2^-$ (eq 11) calculated using the statistical model (eq 4) with three reaction energies: 22 kcal/mol (—), 24 kcal/mol (− − −), and 26 kcal/mol (···). Arrow (↑) indicates the critical energy.

When the accelerated reactant ion (Cl^-) undergoes a collision, the additional kinetic energy is assumed to be incorporated into the internal energy of the reaction system. The total energy of the reaction system is a combination of the center-of-mass collision energy and the thermal internal energy of the neutral reactant. The total energy is then converted to an effective temperature (T_{eff}, defined in the Experimental Section), which is used as an input parameter of the HYDRA program to calculate the statistical efficiency. The corresponding kinetic energy-dependent collision rate constants were calculated with the Su trajectory model. Combining the statistical efficiencies and the energy-dependent collision rate constants, we obtained statistical rate constants at several higher collision energies. The calculated rate constants along with the experimental values are shown in Figure 2a for reaction 10 and in Figure 2b for reaction 11. For both reactions, the observed rate constants agree with the statistical predictions within the energy range examined.

B. Energy Deposition. The statistical internal energy distribution in the ionic S_N2 reaction product was calculated by using the statistical model (eq 4) described in the Experimental Section. For each of the reactions, the excess internal energy at the thermal condition is assumed to be the reaction exothermicity plus the averaged thermal energy of the neutral reactant at 350 K, and the additional kinetic energy is assumed to be incorporated into the internal models of the products. For reaction 11, the exothermicity is 20 kcal/mol, and the averaged thermal energy of $NCCO_2CH_3$ is 2.5 kcal/mol. The combined 22.5 kcal/mol of energy is treated as the excess internal energy distributed statistically over all of the available internal modes of the two products, $NCCO_2^-$ and CH_3Cl. The calculated probability of the energy distribution in $NCCO_2^-$ at a total energy of 22 kcal/mol is plotted in Figure 4. The probable energy in $NCCO_2^-$ is around 13 kcal/mol, and the probabilities of deposition of both 0 and 22 kcal/mol of energy are essentially zero. The critical energy for dissociation of $NCCO_2^-$ to give CN^- is 16.7 kcal/mol. The fraction of $NCCO_2^-$ (F_{stat}) having an internal energy above the dissociation threshold was calculated to be 0.18 (Table 2) by using eq 5. In other words, 18% of the $NCCO_2^-$ produced from reaction 11 could dissociate. As the Cl^- ion translational energy is increased, the total internal energy in the products is increased accordingly. The energy distribution plots for the addition of 2 and 4 kcal/mol (CM) of kinetic energy to Cl^-

(corresponding to the total energies in the reaction systems of 24 and 26 kcal/mol) are also shown in Figure 4. It is obvious that the plot shifts to the higher-energy side as the total energy is increased. By using eq 5, we calculated a series of F_{stat} values at total energies between 22 and 30 kcal/mol. The results are plotted in Figure 3a. At thermal energy, the calculated F_{stat} is comparable to the observed F_{expt}. As the system energy is increased, F_{stat} increases much faster than does F_{expt}.

By using a similar procedure, we calculated F_{stat} for reactions 12 and 13. The exothermicity for reaction 12 is 47 kcal/mol, and the dissociation energy for $CF_3CO_2^-$ to yield CF_3^- is 39.2 kcal/mol. The average thermal energy for $CF_3CO_3CH_3$ at 350 K is 4.3 kcal/mol, giving the thermal F_{stat} of 0.34 (Table 2). A series of F_{stat} values calculated at different system energies are plotted in Figure 3b. Similar to that in Figure 3a, F_{stat} increases significantly as the system energy is increased, while F_{expt} is essentially not changed. A new feature shown in Figure 3b is that even at thermal condition F_{stat} is much larger than the observed F_{expt}. The same feature is also seen in reaction 13. Reaction 13 has a similar exothermicity (50 kcal/mol) to that of reaction 12. The thermal F_{stat} for reaction 13 was calculated to be 0.94 (Table 2), while the observed F_{expt} was 0.4. A series of F_{stat} calculated as a function of energies is plotted in Figure 3c. In this case, both F_{stat} and F_{expt} plots are insensitive to the increase in energies.

Discussion

We have investigated the internal energy distribution in reaction products and kinetic energy effects on reactivity for several exothermic gas-phase S_N2 reactions of halide with methyl esters. These reactions have similar reactants, intermediate complexes, and products but different exothermicities (20−50 kcal/mol) and product ion dissociation energies (17−39 kcal/mol). We want to know whether these reactions behave statistically and what important factors control the observed reaction kinetics and energy distributions.

A. Kinetics. The reaction of $CF_3CO_2CH_3$ with Cl^- (eq 10) has a thermal-reaction rate constant of 0.11×10^{-9} cm^3 molecule^{-1} s^{-1} and a collision rate constant of 2.8×10^{-9} cm^3 molecule^{-1} s^{-1}, giving a reaction efficiency of 0.037. The reaction of $NCCO_2CH_3$ with Cl^- (eq 11) has reaction and collision rate constants of 0.75×10^{-9} and 3.9×10^{-9} cm^3 molecule^{-1} s^{-1}, respectively, and an efficiency of 0.19. Reaction 11 is about 7 times faster than reaction 10. Both the collision rate (1.4 times larger) and efficiency (5 times higher) contribute to the faster rate observed for reaction 11. The larger collision rate constant for reaction 11 comes from the larger dipole moment in $NCCO_2CH_3$ (4 D[54]) compared to that in $CF_3CO_2CH_3$ (3 D[54]).

As shown in Figure 2a and b, both reactions exhibit a negative kinetic energy dependence (i.e., the reactions proceed more slowly as the kinetic energies are increased). The measured rate constants agree with the values calculated with RRKM theory at higher collision energies. The observed negative kinetic energy dependence on reactivity has three origins. First, the ion−dipole capture theory predicts smaller collision rate constants (k_{coll}) at higher collision energies.[55] As shown in eq 7, a smaller collision rate would lead to a smaller overall reaction rate. Second, the overall efficiencies are expected to have a negative energy dependence because of the competition between crossing the central barrier (isomerization) and dissociation back to the reactants. The back dissociation (k_b) has a higher barrier and hence a greater energy dependence than does the isomerization pathway (k_f). The net result is that the term $k_f/(k_f + k_b)$ gets smaller with increasing energy. Third, collisions at increased kinetic energies have larger orbital angular momenta, and the energy tied up in angular rotational energy will be larger for collisions at higher kinetic energy.[11] This situation increases the effective central barrier for the S_N2 reaction. For some cases with larger angular momenta, the effective activation energies may be even higher than the energies of the separated reactants. When this occurs, the overall energy dependence of the rate constant will be positive.[14] However, we did not observe this up-turn of the rate constant within the energy range examined.

The two reactions of F^- with $CF_3CO_2CH_3$ (eq 12) and $NCCO_2CH_3$ (eq 13) are highly exothermic, and the upper-limit reaction efficiencies are close to unity (0.82 for reaction 12 and 0.87 for reaction 13). Higher reaction efficiencies correspond to lower activation energies. As the barrier to reaction becomes smaller, the potential energy surface approaches the limit of a barrierless single-well surface. In this limit, a reaction is expected to occur near the collision rate, and the overall energy dependence of the reaction would primarily reflect the variation in the collision rate.[14] Therefore, the energy dependence on the reaction rate for reactions 12 and 13 is expected to be much smaller, and we did not examine kinetic energy effects on reactivity for these two reactions.

B. Energy Deposition. We probe the internal energy deposition in ionic S_N2 products by measuring the fraction of secondary fragments formed from dissociation of the ionic products. The observed fraction of secondary fragments is compared with the fraction of ionic products having internal energies above dissociation thresholds calculated using a statistical model. As shown in Table 2, the fraction of CN^- observed from reaction 11 is 0.12, and the fraction of internally excited $NCCO_2^-$ is calculated to be 0.18. Calculations show that, if statistical, the fraction of the internally excited $CF_3CO_2^-$ from reaction 12 would be 0.34, while the observed fraction of CF_3^- is only 0.01. Similarly, a fraction of 0.94 of the $NCCO_2^-$ formed from reaction 13 is predicted to be above the threshold, but the observed fraction of CN^- is 0.4. The experimental techniques employed in this study are well established, and the errors associated with the experimental measurements are relatively small (<10%). The errors associated with statistical calculations mainly arise from the uncertainties in the reaction exothermicity and bond dissociation energies. The effects of these uncertainties will be discussed for each reaction. As shown in Figure 3a−c, , as the reactant ion translational energies increase, the fractions of internally excited ionic products increase significantly for both reactions 11 and 12, while the increases in the secondary fragments are much smaller. For reaction 13, both the observed fractions of secondary ions and the calculated fractions of internally excited ionic products are insensitive to the increase in reactant ion translational energies.

Formation of CF_3^- from the reaction of Cl^- with $CF_3CO_2CH_3$ is endothermic by 23 kcal/mol (eq 10a), and we do not observe CF_3^- by adding up to 12 kcal/mol (CM) of kinetic energy to the Cl^- ion. We use this reaction as a control experiment to make sure that the observed secondary fragments from reactions 11, 12, and 13 are not due to artifacts.

The S_N2 reaction of Cl^- with $NCCO_2CH_3$ (eq 11) is exothermic by 20 kcal/mol, and dissociation of $NCCO_2^-$ requires 17 kcal/mol of energy. Therefore, formation of CN^- is exothermic by only 3 kcal/mol (eq 11a). Statistically, 18% of $NCCO_2^-$ would have enough internal energy to dissociate. The amount of CN^- observed corresponds to dissociation of 12% of $NCCO_2^-$. We found that the statistical fraction of hot (internally excited) $NCCO_2^-$ is very sensitive to the reaction

energy. By increasing the reaction energy from 22 to 24 kcal/mol, the statistical fraction of hot $NCCO_2^-$ increases from 0.18 to 0.28. If we were to reduce the reaction energy to 20 kcal/mol, the calculated fraction of hot $NCCO_2^-$ would decrease to 8%. To a first approximation, the fraction of CN^- observed is comparable to the fraction of hot $NCCO_2^-$ with a statistical distribution of thermal internal energy.

It is reasonable that the statistical fraction of hot $NCCO_2^-$ increases significantly as the total excess energy is increased. Both $NCCO_2^-$ and CH_3Cl have the same number of vibrational modes, but $NCCO_2^-$ has more low-energy frequencies. Compared to that for CH_3Cl, the density of states for $NCCO_2^-$ is larger and increases faster at higher energies. As a result, the probability of energy distribution plot for $NCCO_2^-$ (Figure 4) shows a larger population of $NCCO_2^-$ at higher energy. Therefore, even a small amount of additional energy would increase the fraction of hot $NCCO_2^-$ dramatically. Figure 3a shows that the observed fraction of CN^- increases noticeably at increasing kinetic energy but the changes are smaller than the values predicted with the statistical model. Nonetheless, the slight increase in the slope of F_{expt} indicates that at least a small amount of added translational energy is partitioned into the internal modes of the ionic product, $NCCO_2^-$. It is difficult to conclude whether the energy distribution in the ionic product behaves statistically for this reaction.

The reaction of F^- with $CF_3CO_2CH_3$ (eq 12) is exothermic by 47 kcal/mol. Dissociation of $CF_3CO_2^-$ requires 39 kcal/mol of energy, and formation of CF_3^- is exothermic by 8 kcal/mol (eq 12a). However, only 1% of $CF_3CO_2^-$ produces measurable CF_3^-. Statistically, 34% of $CF_3CO_2^-$ has internal energy above the dissociation threshold. Considering that 12% of CN^- is formed in reaction 11a while only 1% of CF_3^- was observed in this reaction, a noticeable barrier above the endothermicity might be involved in the dissociation of $CF_3CO_2^-$. $CF_3CO_2^-$ is undoubtedly a covalent molecule, as opposed to being a complex of CF_3^- and CO_2, and the changes in geometry and electronic structure upon dissociation could result in a barrier. Thus, the actual energy required for dissociation of $CF_3CO_2^-$ would be higher than the endothermicity. A dissociation threshold of 40.1 $\pm$ 4.6 kcal/mol[56] gives an upper limit to the dissociation energy. If we add 3 kcal/mol to the dissociation energy (39.2 kcal/mol) derived using heats of formation, the calculated statistical fraction of hot $CF_3CO_2^-$ decreases from 34% to 15% under thermal conditions. Given the 2 kcal/mol of uncertainty associated with the reaction exothermicity, the change in the calculated fraction of hot $CF_3CO_2^-$ is less than 30%. Combining the uncertainties in both the reaction exothermicity and the bond dissociation energy, the statistical fraction of hot $CF_3CO_2^-$ is still higher than 1% under thermal conditions, indicating that the internal energy deposition in $CF_3CO_2^-$ is much lower than that predicted by the statistical model.

On the other hand, the agreement of the measured and calculated branching ratio for reaction 11 implies that the reverse activation barrier for dissociation of $NCCO_2^-$ is negligible. The low dissociation energy of $NCCO_2^-$ and the ready exchange of CN^- between different neutral molecules (reaction 17, for example) suggest predominately electrostatic bonding in $CN-CO_2^-$ and a productlike transition state for dissociation.[57]

The reaction of F^- with $NCCO_2CH_3$ (eq 13) has similar exothermicity (50 kcal/mol) to that for reaction 12, but dissociation of the ionic product requires much less energy (17 kcal/mol), which leads to 23 kcal/mol of excess energy toward formation of CN^- (eq 13a). The ion $NCCO_2^-$ is expected to be highly internally excited, and a large fraction of $NCCO_2^-$ would have enough energy for dissociation. Indeed, the calculated statistical fraction of hot $NCCO_2^-$ at thermal energy is 0.94. Less than a 5% change in the calculated fraction of hot $NCCO_2^-$ would be obtained by adding 2 kcal/mol of uncertainty to the reaction energy. It is not surprising that the F_{stat} value is not sensitive to the increase in system energy because the maximum value of F_{stat} is 1. It is surprising that the F_{expt} values are only about 40% of the F_{stat} values for the energy range examined (Figure 3c), suggesting that the energy deposition in $NCCO_2^-$ is lower than that predicted by the statistical model. The results from this system also show clearly nonstatistical character in reaction energy deposition.

Reaction 13 is 30 kcal/mol more exothermic than reaction 11. The difference in these two reactions is the same as that for the methyl cation-transfer reaction (eq 20), which has an exothermicity of 31 kcal/mol.[53] Because Cl^- and F^- have similar electron-binding energies, the exothermicity in reaction 20 is mainly the result of the stronger C−F bond. Analogously to reaction 20, the 30 kcal/mol of excess exothermicity in reaction 13 would arise from the stronger C−F bond. Similarly, reaction 12 is more exothermic than reaction 10 by 31 kcal/mol (Table 3), and this excess energy is also due to the formation of the stronger C−F bond. Furthermore, we can see that the excess energy in the S_N2 reaction product complex is directly related to the strength of the newly formed bond in the neutral moiety.

$$F^- + CH_3{-}Cl \rightarrow F{-}CH_3 + Cl^- \qquad (20)$$

According to Hase's energy-transfer model,[16] isomerization of an S_N2 reactant complex leads to an intramolecularly excited product complex in which the excess energy is stored in the vibrational modes of the neutral moiety.[23] Energy is then transferred into intermolecular modes for dissociation to the products. The competition between energy transfer and complex dissociation determines the extent of energy redistribution. If the rate for dissociation is faster than the rate for energy transfer, the complex will dissociate with most of the excess energy trapped in the neutral fragment vibrational modes. Incomplete energy transfer has been inferred from the kinetic energy release distribution (KERD) experiments of the dissociation of metastable complexes, such as $[(CH_3Br)Cl^-]^*$ and $[(CF_3CO_2CH_3)Cl^-]^*$, in which the relative translational energy distributions in the displacement products are lower than the statistical theory predictions.[34−36] Because these reactions are very exothermic (>10 kcal/mol), it is reasonable to expect that the dissociation rates will be fast compared to the speed of energy redistribution. Dissociation of the product complex will occur as soon as the minimum amount of energy has been transferred to the dissociation reaction coordinate. Thus, the dissociating products will have essentially no additional kinetic energy. This process is analogous to the activation of unimolecular reactions in the low-pressure limit, where the reaction occurs as soon as the critical energy has been reached so that the energy of molecules undergoing reaction is less than that observed at high pressure.[58] The nonstatistical product energy distribution for the reaction of Cl^- with CH_3Br has also been shown by trajectory calculations, in which the vibrational energy distribution in CH_3Cl is higher while the relative translational energy distribution is lower than the statistical theory predictions.[16,23]

While a nonstatistical translational energy distribution indicates a bottleneck to T $\leftrightarrow$ V energy transfer in the S_N2 product complex, the nonstatistical internal energy deposition observed in our study implies a bottleneck to intermolecular V $\leftrightarrow$ V energy transfer in the product complex. The lower fractions of CF_3^- and CN^- observed in reactions 12 and 13 indicate that

internal energy depositions in the ionic S_N2 products, $CF_3CO_2^-$ and $NCCO_2^-$, are much lower than those predicted by the statistical model. As discussed above, most of the excess energy in the product complexes, $(CF_3CO_2^-)CH_3F$ and $(NCCO_2^-)CH_3F$, comes from the newly formed C−F bonds. The product complexes are initially formed with CH_3F vibrationally hot and $CF_3CO_2^-$ and $NCCO_2^-$, cold. The energy stored in CH_3F must flow into the vibrational modes of $CF_3CO_2^-$ and $NCCO_2^-$ to produce secondary ionic fragments. Collisional relaxation experiments suggest that energy transfer from vibrationally excited $CF_3CO_2^-$ to a variety of neutral collision molecules is inefficient.[59] Studies also show strong correlation between the extents of energy transfer and RRKM lifetimes of the collision complexes. The energy transfer efficiencies are larger for long-lived complexes and smaller for short-lived ones. Because reactions 12 and 13 are highly exothermic (47−50 kcal/mol), the product complexes will have short lifetimes because of the fast dissociations. Therefore, incomplete V ↔ V energy transfer is expected, and the excess energy will be trapped in CH_3F upon dissociation, leaving $CF_3CO_2^-$ and $NCCO_2^-$ vibrationally cold.

As the exothermicity is decreased, the lifetime of the product complex will be longer, and V ↔ V energy transfer is expected to be more efficient. Such a case is seen in reaction 11, in which the energy deposition in the ionic product is comparable to the statistical value at the thermal condition. The relatively lower energy deposition observed at higher collision energies may due to the inefficient T ↔ V energy transfer upon collision. Previous experimental results of the dissociation of the *tert*-butoxide-d_6 anion using the ion kinetic energy controller suggest that kinetic to internal energy transfer is very inefficient.[38] Collision of the kinetically accelerated (about 100 kcal/mol, CM) *tert*-butoxide-d_6 anion with argon produced fragment ions with a large secondary isotope effect. The estimated average energy transferred per collision is 2 kcal/mol, suggesting an energy transfer efficiency of about 2% per collision. While energy transfer may be more efficient at lower collision energies,[60] the amount of energy transferred into the internal modes of $NCCO_2CH_3$ is expected to be smaller than the additional kinetic energy added to Cl^-.

Conclusions

We have investigated internal energy deposition in reaction products and kinetic energy effects on reactivity for several exothermic S_N2 reactions of halides with methyl esters. Rate constants for the reactions of Cl^- with $CF_3CO_2CH_3$ and $NCCO_2CH_3$ were measured as a function of increasing Cl^- translational energies. A negative kinetic energy dependence was observed for both reactions. Statistical rate constants were calculated using RRKM theory. The measured rate constants as a function of kinetic energy agree with the RRKM theory predictions.

Internal energy deposition in the S_N2 products was examined for the reactions of Cl^- with $NCCO_2CH_3$ and F^- with $CF_3CO_2CH_3$ and $NCCO_2CH_3$ by measuring the fraction of secondary fragments resulting from the dissociation of internally excited S_N2 product ions. We have developed a statistical model to calculate the statistical energy distribution in S_N2 products. The results from the experiments are compared with those calculated using the statistical model. For the least exothermic reaction (<20 kcal/mol), the measured internal energy deposition in the ionic product is comparable to that calculated using the statistical model at the thermal condition. For a highly exothermic reaction (>40 kcal/mol), the internal energy deposition in the ionic product is significantly lower than the statistical value, indicating that most of the excess energy is trapped in the neutral fragment. Additional translational energy has little effect on the observed fraction of secondary ions. The nonstatistical internal energy distribution in the S_N2 products implies a bottleneck to intermolecular vibrational energy transfer within the product complex.

Acknowledgment. This work was supported by the National Science Foundation. We thank Dr. Stephen Craig for helpful discussions on using the ion trajectory model that he developed to calculate ion kinetic energies.

Supporting Information Available: Selected calculated optimized geometries, energies, vibrational frequencies, and rotational constants. This material is available free of charge via the Internet at http://pubs.acs.org.

References and Notes

(1) Shaik, S. S.; Schlegel, H. B.; Wolfe, S. *Theoretical Aspects of Physical Organic Chemistry: The S_N2 Mechanism*; Wiley & Sons: New York, 1992.
(2) Moylan, C. R.; Brauman, J. I. In *Advances in Classical Trajectory Methods*; JAI Press Inc.: 1994; Vol. 2, pp 95−114.
(3) Olmstead, W. N.; Brauman, J. I. *J. Am. Chem. Soc.* **1977**, *99*, 4219−4228.
(4) Pellerite, M. J.; Brauman, J. I. *J. Am. Chem. Soc.* **1979**, *102*, 5993−5999.
(5) Wladkowski, B. D.; Lim, K. F.; Allen, W. D.; Brauman, J. I. *J. Am. Chem. Soc.* **1992**, *114*, 9136−9153.
(6) Wolfe, S.; Mitchell, D. J. *J. Am. Chem. Soc.* **1981**, *103*, 7694−7696.
(7) Wladkowski, B. D.; Wilbur, J. L.; Brauman, J. I. *J. Am. Chem. Soc.* **1994**, *116*, 2471−2480.
(8) Li, C.; Ross, P.; Szulejko, J. E.; McMahon, T. B. *J. Am. Chem. Soc.* **1996**, *118*, 9360−9367.
(9) Wilbur, J. L.; Brauman, J. I. *J. Am. Chem. Soc.* **1994**, *116*, 9216−9221.
(10) Baer, T.; Hase, W. L. *Unimolecular Reaction Dynamics: Theory and Experiments*; Oxford University Press: New York, 1996.
(11) Gilbert, R. G.; Smith, S. C. *Theory of Unimolecular and Recombination Reactions*; Blackwell Scientific: Oxford, 1990.
(12) Forst, W. *Theory of Unimolecular Reactions*; Academic Press: New York, 1973.
(13) Robinson, P. J.; Holbrook, K. A. *Unimolecular Reactions*; Interscience: London, 1972.
(14) Craig, S. L.; Zhong, M.; Brauman, J. I. *J. Am. Chem. Soc.* **1999**, *121*, 11790−11797.
(15) Hase, W. L. *Acc. Chem. Res.* **1998**, *31*, 659−665.
(16) Hase, W. L. *Science* **1995**, *266*, 998−1002.
(17) Tonner, D. S.; McMahon, T. B. *J. Am. Chem. Soc.* **2000**, *122*, 8783−8784.
(18) Viggiano, A. A.; Morris, R. A.; Paschkewitz, J. S.; Paulson, J. F. *J. Am. Chem. Soc.* **1992**, *114*, 10477−10482.
(19) Viggiano, A. A.; Morris, R. A. *J. Phys. Chem.* **1996**, *100*, 19227−19240.
(20) Wang, H.; Hase, W. L. *J. Am. Chem. Soc.* **1997**, *119*, 3093−3102.
(21) Wang, H.; Hase, W. L. *J. Am. Chem. Soc.* **1995**, *117*, 9347−9356.
(22) Wang, H.; Hase, W. L. *Chem. Phys.* **1996**, *212*, 247−258.
(23) Wang, H.; Peslherbe, G. H.; Hase, W. L. *J. Am. Chem. Soc.* **1994**, *116*, 9644−9651.
(24) Craig, S. L.; Zhong, M.; Brauman, J. I. *J. Am. Chem. Soc.* **1998**, *120*, 12125−12126.
(25) Cho, Y. J.; Linde, S. R. V.; Zhu, L.; Hase, W. L. *J. Phys. Chem.* **1992**, *96*, 8275−8287.
(26) Viggiano, A. A. et al. *J. Am. Chem. Soc.* **1994**, *116*, 2213−2214.
(27) Basilevsky, M. V.; Ryaboy, V. M. *Chem. Phys. Lett.* **1986**, *129*, 71−75.
(28) Hase, W. L.; Wang, H.; Peslherbe, G. H. *Adv. Gas Phase Ion Chem.* **1998**, *3*, 125−156.
(29) Ryaboy, V. M. *Chem. Phys. Lett.* **1989**, *159*, 371−374.
(30) Knighton, W. B.; Bognar, J. A.; O'Connor, P. M.; Grimsrud, E. P. *J. Am. Chem. Soc.* **1993**, *115*, 12079−12084.
(31) DeTuri, V. F.; Hintz, P. A.; Ervin, K. M. *J. Phys. Chem. A* **1997**, *101*, 5969−5986.
(32) Morris, R. A.; Viggiano, A. A. *J. Phys. Chem.* **1994**, *98*, 3740−3746.
(33) Craig, S. L.; Brauman, J. I. *Science* **1997**, *276*, 1536−1538.

(34) Graul, S. T.; Bowers, M. T. *J. Am. Chem. Soc.* **1991**, *113*, 9696−9697.
(35) Graul, S. T.; Bowers, M. T. *J. Am. Chem. Soc.* **1994**, *116*, 3875−3883.
(36) Graul, S. T.; Carpenter, C. J.; Bushnell, J. E.; van Koppen, P. A. M.; Bowers, M. T. *J. Am. Chem. Soc.* **1998**, *120*, 6785−6796.
(37) Van Orden, S. L.; Pope, R. M.; Buckner, S. W. *Org. Mass Spectrom.* **1991**, *26*, 1003−1007.
(38) Boering, K. A.; Rolfe, J.; Brauman, J. I. *Int. J. Mass Spectrom. Ion Processes* **1992**, *117*, 357−386.
(39) Wilbur, J. L. Ph.D. Dissertation, Stanford University, Stanford, CA, 1993.
(40) Han, C.-C.; Brauman, J. I. *J. Am. Chem. Soc.* **1989**, *111*, 6491−6496.
(41) McIver, J. R. T. *Int. J. Mass Spectrom. Ion Processes* **1989**, *89*, 343−358.
(42) Kemper, P. R.; Bowers, M. T. In *Techniques for the Study of Ion−Molecule Reactions*; Farrar, J. M., Saunders, W. H., Jr., Eds.; Wiley-Interscience: New York, 1988; Vol. 20, p 17.
(43) Grosshans, P. B.; Shields, P.; Marshall, A. G. *J. Am. Chem. Soc.* **1990**, *112*, 1275−1277.
(44) Guan, S.; Marshall, A. G. *Int. J. Mass Spectrom. Ion Processes* **1996**, *157−158*, 5−37.
(45) Craig, S. L.; Brauman, J. I. *J. Phys. Chem. A* **1997**, *101*, 4745−4752.
(46) Craig, S. L.; Brauman, J. I. *Ber. Bunsen-Ges. Phys. Chem.* **1997**, *101*, 510−515.
(47) Frisch, M. J.; Trucks, G. W.; Schlegel, H. B.; Scuseria, G. E.; Robb, M. A.; Cheeseman, J. R.; Zakrzewski, V. G.; Montgomery, J. A., Jr.; Stratmann, R. E.; Burant, J. C.; Dapprich, S.; Millam, J. M.; Daniels, A. D.; Kudin, K. N.; Strain, M. C.; Farkas, O.; Tomasi, J.; Barone, V.; Cossi, M.; Cammi, R.; Mannucci, B.; Pomelli, C.; Adamo, C.; Clifford, S.; Ochterski, J.; Petersson, G. A.; Ayala, P. Y.; Cui, Q.; Morokuma, K.; Malick, D. K.; Rabuck, A. D.; Raghavachari, K.; Foresman, J. B.; Cioslowski, J.; Ortiz, J. V.; Stefanov, B. B.; Liu, G.; Liashenko, A.; Piskorz, P.; Komaromi, I.; Gomperts, R.; Martin, R. L.; Fox, D. J.; Keith, T.; Al-Laham, M. A.; Peng, C. Y.; Nanayakkara, A.; Gonzalez, C.; Challacombe, M.; Gill, P. M. W.; Johnson, B. G.; Chen, W.; Wong, M. W.; Andres, J. L.; Head-Gordon, M.; Replogle, E. S.; Pople, J. A. *Gaussian 98*; Gaussian, Inc.: Pittsburgh, PA, 1998.
(48) Weyssenhoff, H. v.; Schlag, E. W. *J. Chem. Phys.* **1973**, *59*, 729−740.
(49) Beyer, T.; Swinehart, D. F. *Comm. Assoc. Comput. Machines* **1973**, *16*, 379.
(50) Wladkowski, B. D.; Lim, K. F.; Brauman, J. I. *HYDRA: Calculation of Ion−Molecule Reaction Rate Coefficients Using Variational Transition State Theory*; 1991.
(51) Su, T. *J. Chem. Phys.* **1994**, *100*, 4703.
(52) Larson, J. W.; Szulejko, J. E.; McMahon, T. B. *J. Am. Chem. Soc.* **1988**, *110*, 7604−7609.
(53) *NIST Chemistry Webbook, NIST Standard Reference Database Number 69*; Mallard, W. G., Lindstrom, P. J., Eds. National Institute of Standards and Technology: July 2001.
(54) Values obtained from MP2/6-31G(d) calculations.
(55) Su, T.; Bowers, M. T. In *Gas-Phase Ion Chemistry*; Bowers, M. T., Ed.; Academic Press: New York, 1979; Vol. 1, pp 83−119.
(56) Graul, S. T.; Squires, R. R. *J. Am. Chem. Soc.* **1990**, *112*, 2517−2529.
(57) Larson, J. W.; McMahon, T. B. *J. Am. Chem. Soc.* **1988**, *110*, 7604−7609.
(58) Wilbur, J. L.; Wladkowski, B. D.; Brauman, J. I. *J. Am. Chem. Soc.* **1993**, *115*, 10823−10829.
(59) Boering, K. A.; Brauman, J. I. *J. Chem. Phys.* **1992**, *97*, 5439−5449.
(60) Wysocki, V. H.; Kenttamaa, H. I.; Cooks, R. G. *Int. J. Mass Spectrom. Ion Processes* **1987**, *75*, 181−208.